NONLINEAR DYNAMIC AND CREEP BUCKLING OF ELLIPTICAL PARABOLOIDAL CONCRETE SHELLS

Porfirio Ballesteros

Sección de Estructuras
Enero de 1978

4

UNIVERSIDAD NACIONAL AUTONOMA DE MEXICO

NONLINEAR DYNAMIC AND CREEP BUCKLING OF ELLIPTICAL PARABOLOIDAL CONCRETE SHELLS

By

Porfirio Ballesteros[1]

SUMMARY

The collapse of some elliptical paraboloidal concrete shells at some country is studied considering nonlinearity in geometry, material, and creep response. In the shell geometry the effect of the imperfections on the critical pressure is taken into account. From the theoretical considerations, and the data obtained from the collapse of this kind of shell, important design recomendations are proposed.

INTRODUCTION

Last september, 1975, the author was consulted from some country to study the motive of the collapse of elliptical paraboloidal concrete shells whose geometry is shown in Figs 2 and 3.

The following information from the prototype was obtained:

a) The collapse happened in-between ninety and one hundred hours after the concrete forwork was removed, figs 9 and 10.

b) The unconfined compressive strength of the concrete in the structure was $f'_c \leq 150\ kg/cm^2$ (2000 psi).

c) Very significant geometric imperfections of the formwork were observed, Fig 11.

---

1 Chairman Structural Mechanics, Graduate Division, School of Engineering, National University of Mexico.

d) An earthquake with considerable vertical component happened during the collapse.

e) The day-laborers of the construction reported deflections at the apex of an order of magnitude of 15.00cm (6 inches), before the collapse.

f) The deflection at the apex, measured in the existing shells, one day after removing the formwork, was of an order of magnitude of 9.00cm (3.5 inches). So the author's instructions were to shore immediately the shells which had not collapsed yet, to avoid possible problems.

Based on this information, the collapse of course was originated by an elastic-plastic dynamic buckling with creep response.

PRACTICAL CONSIDERATIONS

The problem of giving a practical solution with the objective of saving the existing shells and to be able to continue the construction, was studied and, so, the following computation and solution was presented.

a) Buckling capacity of the shells.

The buckling pressure p_{cr}, of this kind of shells is given by [19]

$$p_{cr} = CE \frac{t^2}{R_1 R_2}$$

where for concrete shells, $0.05 \leq C \leq 0.15$, and from Fig.2. In our case we have $R_1 = 32.90m$, $R_2 = 33.57m$, $t = 0.06m$, and $E \doteq 150\ 000\ kg/cm^2$. Substituting in (a) for the lower limit of C, we have

$$p_{cr} = 244.5 \ \frac{kg}{m^2} \qquad (b)$$

The dead weight and live load of the shell were:

$$w \doteq \gamma t = 0.06 \times 2400 = 144.00 \ kg/m^2 \qquad (c)$$

and the live load; $p = 100 \ kg/m^2$ (d)

comparing (c) and (d) with (b) we have

$$\frac{p_{cr}}{w+p} = \frac{244.5}{144 + 100} \leq 1, \qquad \frac{p_{cr}}{w} = \frac{244.5}{144} \leq 1.7 \qquad (e)$$

So the shells had a very low buckling capacity

b) Increasing the buckling capacity of the existing shells by additional arches

The buckling of a circular arch is given by [20]

$$q_{cr} = \frac{EI_z}{r^3} \left(\frac{\pi^2}{\alpha^2} - 1\right) \qquad (f)$$

using an arch of, $f_c' = 300 \ kg/cm^2$, $E = 260\ 000 \ kg/cm^2$, $I_z = 106\ 000 cm^4$, $r = 33.00m$, and $\alpha = 0.55$ radians, from (f) we obtain, $q_{cr} = 2400 \ kg/m$. The arches were connected to the shells in the way shown in Figs 12,13,14,15,16,17,18 and 19. The increase of the tension in the perimetral ties was 7.4 Ton, and it was not necessary to put any additional reinforcement.

c) Field load test.

After the arches were connected to the shells, a static field load test was carried on two of the shells applying a load of $2.4\ (w+p) = 585.6\ kg/m^2$; the shell was loaded in 24 hours and stayed during 360 hours, the deflection at the apex reaching maximum value of 3.8cm (1.5 inches) in 48 hours with respect to time in which the loading manoeuvre started. After 360 hours the shell was unloaded and the deflection at the apex recovered its 100%. The reinforcement details of the arches is shown in Fig. 13, and 14.

THEORETICAL CONSIDERATIONS

a) Linearly Elastic-plastic strain hardening-fracture material

The analytical constitutive relation of concrete under general three-dimensional stress state has already been proposed [1,2]. In the formulation, the concrete is assumed to be a continuous, isotropic, and linearly elastic-plastic strain hardening-fracture material. The elastic-plastic stress-strain incremental relationships, based on the initial discontinuous surface, loading surfaces, and failure surface of concrete are derived using the classical theory of plasticity. For the special case of a biaxial stress-strain relationship for a concrete shell under a plane stress condition, the constitutive relationships are

$$\begin{Bmatrix} dN_x \\ \\ dN_y \\ \\ dN_{xy} \end{Bmatrix} = \frac{Et}{1-\nu^2} \begin{bmatrix} 1-\omega\phi_{11} & \nu-\omega\phi_{12} & -\omega\phi_{13} \\ \\ & 1-\omega\phi_{22} & -\omega\phi_{23} \\ \\ & & \frac{1-\nu}{2}-\omega\phi_{33} \end{bmatrix} \begin{Bmatrix} d\varepsilon_X \\ \\ d\varepsilon_Y \\ \\ d\varepsilon_Z \end{Bmatrix} \tag{1}$$

where we have denoted

$$\frac{1}{\omega} = \left[2(1-\nu)J_2 - (1-2\nu)S_{33}^2 - 2(1-\nu)\rho\, S_{33} + 2(1+\nu)\rho^2\right.$$

$$\left. + \frac{H\,(1-\nu^2)}{E}\sqrt{2J_2+2\rho^2}\,(1-\frac{\alpha}{3}I_1)\right]$$

$$\phi_{11} = \left[(1-\nu)S_{11} - \nu S_{33} + (1+\nu)\rho\right]^2$$

$$\phi_{12} = \left[(1-\nu)S_{11} - \nu S_{33} + (1+\nu)\rho\right]\left[(1-\nu)S_{22} - \nu S_{33} + (1+\nu)\rho\right] \tag{2}$$

$$\phi_{13} = \left[(1-\nu)S_{11} - \nu S_{22} + (1+\nu)\rho\right]\left[(1-\nu)\tau_{12}\right]$$

$$\phi_{22} = \left[(1-\nu)S_{22} - \nu S_{33} + (1+\nu)\rho\right]^2$$

$$\phi_{23} = \left[(1-\nu)S_{22} - \nu S_{33} + (1+\nu)\rho\right]\left[(1-\nu)\tau_{12}\right]$$

$$\phi_{33} = \left[(1-\nu)\tau_{12}\right]^2$$

in which ν = Poisson's ratio; E = Young's modulus; $S_{ij}=\sigma_{ij}-\delta_{ij}I_1/3$ the stress deviator tensor; τ_{ij} = material constant; and $\rho = n\, I_1 + \frac{(\alpha+\beta\tau_{ij}^2)}{2}$, in which n=0 when stress state is lying in the compression zone and -1/3 in the tension zone; α and β are parameters, I_1 is the first invariant of the stress tensor, H is the strain-hardening rate function, and J_2 is the second invariant of S_{ij}.

b) Linearly viscoelastic material.

The theory of linear viscoelasticity for infinitesimal deformations is well known and has been applied to several boundary-value problems. The response σ_{ij} to a given history $\varepsilon_{ij}(t)$ is given in [4] by the convolution integral

$$\sigma_{ij}(t) = G_{ijkl}(t)\, E_{kl}(0) + \int_0^{t'} G_{ijkl}(t-t')\, \frac{d}{dt'}\, \varepsilon_{kl}(t)dt' \quad (3)$$

where ε_{ij} and σ_{ij} are the infinitesimal strain and the stress, respectively. The integrating function G_{ijkl} reduces it to two independent components for isotropic materials and exhibits its fading memory.

The most general nonlinear theory gives the free energy as a functional of the strain history and derives the stress response from it, which its numerical solution increases the computational time. Equation (3) was derived for the case for a linear constitutive equation; however, the kinematics of the deformation is nonlinear. In [5] a generalization of Eq. (3) is given but computationally it is not convenient, so in [6,7] an alternative formulation using convected coordinates has been used in this problem.

In order to avoid transformation to physical tensor components, in

[4] is given a pure Lagrangian generalization of (3) where the symmetric stress and strain tensors are used, and (3) is interpreted as a functional relationship between their physical components, and it becomes

$$'S_{IJ}(t_1) = G_{IJKL}(t_1)E_{KL}(0) + \int_0^{t_1} G_{IJKL}(t_1-t')\,\frac{d}{dt'}E_{KL}(t')dt' \quad (4)$$

where $'S_{IJ}$ is the stress configuration in the current configuration V_1 at time t_1, and $E_{KL}(t')$ is the total Lagrangian strain at time t', but here the material characterization is done by a double power law [3], in which the dependence of creep on load duration (t-t') as well as age at loading t' is described by the law

$$J(t,t') = \frac{1}{E_o}\left[1 + \phi_1(t')^{-m}(t-t')^n\right] \quad (5)$$

in which m, n, ϕ_1 and E_o are material parameters determined from test data by optimization techniques. The law is limited to basic creep, but with different values of material parameters it can also describe drying creep up to a certain time.

J(t,t') represents strain in time t caused by a constant unit stress that has been acting since time t'. Time t' is measured from various tests which are listed in table I, where only short-time creep data up to one month duration is available.

TABLE I (Ref. 3)

Data from	m	n	ϕ_1	$E_o \times 10^6$ psi
1. L'Hermite et al. (in water)	0.221	0.094	3.74	0.0788
2. Dworshak Dam (sealed)	0.355	0.056	17.51	0.0844
3. Ross Dam (sealed)	0.457	0.130	2.80	0.1885
4. Shasta Dam (sealed)	0.536	0.134	5.38	0.1806
5. Canyon Ferry Dam (sealed)	0.295	0.119	4.02	0.1000
6. Gamble and Thomas (RH 94%)	0.450	0.081	4.87	0.1800
7. A.D. Ross (RH 93%)	0.238	0.126	1.97	0.1030
8. L'Hermite et al (BH 50%)	0.213	0.131	11.26	0.0521

From table I we may consider

$$m \doteq \frac{1}{3}, \quad n \doteq 1/8 \tag{6}$$

It has been shown previously in [3] that the creep analysis of large finite element systems is simplified by expanding J(t,t') into Dirichlet series, or exponentials series of the following form:

$$J(t,t') = \frac{1}{E(t')} + \sum_{\mu-1} \frac{1}{\hat{E}_\mu(t')}\left(1-e^{-[(t-t')/\tau_\mu]}\right) \tag{7}$$

where $\{\tau_\mu\}$ are chosen retardation times and $\{\hat{E}_\mu\}$ are material coefficients. This series approximates very closely the double power law in the time interval $0,3\tau_1 \leq t-t' \leq 0.5\ \tau_N$ when one sets $\tau_\mu = 10^{\mu-1}\tau_1 (\mu=1,2,...,N)$ and uses the following expressions:

$$\frac{1}{E(t')} = \frac{1}{E_o} + a(n)\ \left(\frac{\tau_1}{0.002}\right)^n \frac{\phi_1}{E_o} (t')^{-m} \qquad (8)$$

For $\mu<N$

$$\frac{1}{\hat{E}_\mu(t')} = b(n)\left(\frac{\tau_1}{0.002}\right)^n \frac{\phi_1}{E_o}\ 10^{n(\mu-1)} (t')^{-m} \qquad (9)$$

For $\mu = N$

$$\frac{1}{\hat{E}_\mu(t')} = 1.2\ b(n)\ \left(\frac{\tau_1}{0.002}\right)^n \frac{\phi_1}{E_o}\ 10^{n(N-1)} (t')^{-m} \qquad (10)$$

in which τ_1 and t' must be substituted in days, and a(n) and b(n) are coefficients given by Table II. The values of a(n) and b(n) have been obtained by a nonlinear optimization technique (Marquardt algorithm) for sum-of-squares problems.

TABLE II

DIRICHLET SERIES EXPANSION COEFFICIENTS

N	a(n)	b(n)
0.05	0.6700	0.0819
0.10	0.4456	0.1161
0.15	0.2929	0.1229
0.20	0.1885	0.1152
0.25	0.1154	0.1007
0.30	0.0611	0.0842
0.35	0.0156	0.6810

c) *Solution Procedure*

The basic equations for nonlinear finite element analysis are well known for the nonlinear dynamic case. From the principle of virtual work in terms of the initial configuration, one obtains

$$\int_{V_o} [N]^T [\rho] [N] \{\ddot{u}\} dV_o = -\int_{V_o} [B] \{\sigma\} dV_o + \{P\} \tag{11}$$

where $[N]$ is an interpolation function that transforms displacements at the nodes to displacements at any point within the element.

$[B]$ is the transformation matrix that transforms displacement rates at the nodes to strain rates at any point in an element

$\{\sigma\}$ is the generalized stress vector

$[\rho]$ is the density matrix (the density takes on its matrix form in problems of shells)

The equation may now be linearized writing it in its incremental form:

$$\int_{V_o} [N]^T [\rho] [N] dV_o \Delta\{\ddot{u}\} = -\int_{V_o} \Delta [B] \{\sigma\} dV_o - \int_{V_o} [B] \Delta\{\sigma\} dV + \Delta\{P\}$$

$$+ 0(I) + 0(t^m) \tag{12}$$

In the above Eq, $\Delta\{P\}$ should be understood to include the effects of following loads. The two error terms $0(t^m)$ and $0(I)$ are also included to show that the solution in incremental form contains a discretization error due to the current increment as well as an inherited error due to all previous increments. The error due to discretization in time is shown as a function of time raised to the power m.

We now make use of the linearized incremental stress-strain relations which are written as

$$\Delta\{\sigma\} = [D]\Delta\{e\} \tag{13}$$

This equation is appropriate for elastic-plastic behavior and has been outlined for small strain in [10] and for large strains in [11].

Substituting (13) in (12) results in a linearized incremental equation

$$[M]\ \Delta\ \{\ddot{\mu}\} = -\ [k]\ \Delta\ \{\mu\} + \Delta\ \{P\} + 0(t^m) + 0(I) \tag{14}$$

This equation can be specialized to the static case by neglecting the term on the left. In the static case convergence to the true solution may be achieved by applying the load in increasingly smaller increments. A parallel procedure was investigated for the dynamic case where the rate of convergence with decrease in time step was examined.

We now consider the error term 0(I) called the residual load correction, that consists of writing the residual equation for (11)

$$0(I) = -\ [M]\{\ddot{\mu}\} - \int_{V_o} [B]\{\sigma\}dV_o + \{P\} \tag{15}$$

It is noted that this error term consists in evaluating the terms at the state before the current increment and that if no numerical errors had been introduced by previous increments the error would be equal to zero.

It was shown in [4] that, including the residual load correction in the dynamic equations, one may obtain convergent solutions using time increments relatively large in comparison with the solutions obtained without the correction.

The selection of an integration scheme for the solution of the incremental equations in the time domain is critical with respect to computational efficiency. A suitable solution scheme, which allows a large time step and yet gives an accurate solution is that developed by Houbolt [12]. The Houbolt scheme is based on the backwards difference expression

$$\Delta\{\ddot{\mu}\}_n = \frac{1}{\Delta t^2}\{2\Delta\mu_{n-5}\Delta\mu_{n-1}+4\Delta\mu_{n-2}-\Delta\mu_{n-3}\}$$

Applying this to the condition for incremental equilibrium (4) yields

$$(2[M] + \Delta t^2\ [K_n])\Delta\ \{\mu_{n+1}\} = \Delta\{P_{n+1}\}\Delta t^2$$

$$+\ [M]\ (5\Delta\{\mu_n\} - 4\Delta\{\mu_{n-1}\} + \Delta\{\mu_{n-2}\}) + 0(I_n)\Delta t^2$$

where n, is a subscript denoting the time at which the increment is taken. This equation is solved for the displacement increment $\Delta\{\mu_{n+1}\}$ at each step except for the first, where a special starting procedure must be employed [12].

d) Solution Convergence

Haisler et al. [13] have reported on studies of numerical integration schemes and their convergence properties in the nonlinear static case. It was shown there that the incremental finite element formulation gave statisfactory results when the load increments used were small as compared to those adopted in the solutions using the residual load correction term. The nature of the correction procedure was illustrated in [8], where the order of the error for the corrected and uncorrected equations are examined. The result was given for a one-dimensional model and serves to give an order of magnitude estimate of the error.

In the static case for the solution without the residual load correction and a slowly varying stiffness K, the total discretization error is the sum of the truncation errors for each increment of the incremental approximation. This error may be expressed as

$$\mu_N - \mu^*_N = -\frac{1}{2}\sum_{n=2} K^{-1}_{n-1}\frac{dK_{n-1}}{d\mu}\Delta\mu^2_n + 0(\Delta\mu^3) \qquad (16)$$

where μ_n is the correct total displacement after N load increments and μ^*_N is the displacement obtained by the incremental approach. It is noted that the error is $0(\Delta\mu^3)$ in the displacement increment. When the residual load correction is included, we find that,

$$\mu_N - \mu^c_N = -\frac{1}{2} K^{-1}_{N-1}\sum_{n=2}^{\frac{N}{2}+1}\frac{dK_\ell}{d\mu}\Delta\mu^2_K + 0(\Delta\mu^3) \qquad (17)$$

where, for N even, $\ell = m - 1$, $k = m$, and, for N odd, $\ell = m$, $k=m+1$, m being equal to $2(\frac{2n-1}{2})$, and fractions are discarded in the computation of the indexes. Eq. (17) may be described by stating that for even N only terms involving even displacement increments remain in the series and likewise for odd N and odd displacement. In comparing (16) and (17) we see that the inclusion of the residual load correction reduces the number of terms in the series by a half. One could state that, approximately speaking, the error is halved in the corrected equations except for the fact that the stiffness quantity is inside the summation sign in [16]. The assumption of a slowly varying stiffness K in [6] means the neglection of errors caused by the inherited error terms.

In the dynamic case the expressions for the discretization errors of the uncorrected and corrected equations at time $N\Delta t$ are, respectively,

$$u_N - u_N^* = -\frac{\Delta t^2}{4} M^{-1} \left\{ \sum_{n-2}^{N} \left[R_{n-1} \frac{dK_{n-1}}{du} \Delta u_n^2 \right] + E^* \right\} + 0(\Delta u^3) + 0(\Delta t^4) \quad (18)$$

and

$$u_N - u_N^c = -\frac{\Delta t^2}{4} M^{-1} \left\{ R_{N-1} \sum_{n=2}^{\frac{N}{2}+1} \left[\frac{dK}{du} \Delta u_K^2 \right] + E^c \right\} + 0(\Delta u^3) + 0(\Delta t^4) \quad (19)$$

where $R_n = (1 - \frac{\Delta t^2}{2} M^{-1} K_n)$. In the above equations E^* and E^c are the truncation errors inherited from the inertia terms and, for the integration scheme in time, do not appear to be expressible in a general form. However, they are of the same order as the first terms in brackets in (18) and (19), and it is interesting to speculate that a similar reduction in the error occurs in E^c as compared with E^*.

It has been demonstrated in [13] that the static solutions given by the corrected and uncorrected equations, tend to converge as the number of load increments in the uncorrected case are increased. A particular example given in [13] is a spherical shell cap under a point load at the apex where the uncorrected solution converged using an increment one eighth of that which was required for convergence in the corrected solution. One would expect that judging from (18) and (19), the convergence rate in the dynamic case would be more rapid both for the corrected and uncorrected solutions considering the presence of the factor Δt^2, and the fact that the truncation errors for the static and dynamic solutions are approximately of the same order. In the sample problems, mentioned later, it has been shown for the example of a beam under a half-sine wave impulse over the span, that the uncorrected solution converges rapidly as time increment is varied. On the other hand, the corrected solution changes very little over a range of time increments. It appears that with the reduced truncation error of the corrected equations the effect of Δt^2 on the solution is diminished.

The advantage in using the corrected dynamic equations is that one may obtain practically convergent results with large time increments. In the numerical examples mentioned later it was shown that convergent solutions to dynamic problems using the corrected incremental equations may be obtained using time increments of an order of magnitude greater than those used by other investigators. The other solutions were obtained by using the Houbolt scheme and the total form of the finite element equations, so the comparisons are direct. This fact has important consequences in terms of solving nonlinear problems economically.

COMPUTER PROGRAM

The system of equations for the dynamic elastic-plastic analysis with large displacement have been incorporated to a general purpose computer program. A program previously developed at Marc Analysis Research Corporation, Palo Alto, California called MARC program was used as the basic. Figure 1 gives a flow diagram of the procedure.

CASE STUDIES

Several examples were selected by Marcal from [8,9] in order a) to make comparisons with results in the literature, b) to investigate the limits of numerical approximations in terms of the frequency of reassembly and residual load correction, and c) to observe the effect of geometric imperfections in a dynamically loaded sphere.

The one-dimensional element used in this examples is of the isoparametric type and has a rapid rate of convergence even for small numbers of elements. This is due to the fact that it can represent exactly all the rigid body modes of the interpolated surface which is arbitrarily close to the actual structural shape. It has proved to be a very accurate and economic element for use in the analysis of dynamic problems.

The chosen examples are;

1. *Shallow spherical cap under a step pressure load*
2. *Nonlinear elastic analysis of a simply-supported beam under a half-sine initial velocity distribution*
3. *Nonlinear elastic analysis of a spherical shell cap under a point load at the apex*
4. *Elastic-plastic beam under a uniform initial velocity over a*

portion of the Span

5. *Elastic-plastic buckling of an imperfect sphere under a uniform constant external pressure*

NUMERICAL RESULTS

a) *Post-buckling behavior of the shallow concrete elliptical paraboloidal shell with an elliptical imperfection.*

The geometry of this shell is shown in Figs 2 and 3 where the imperfection is given as a flat elliptical section of the shell of radius r_1 and r_2, which are the mean radius of the oblate portion of the elliptical paraboloidal surface.

For the simplest elements, where only displacement continuity is required at the nodes, as in [14] and [15], the intersection between the imperfection and the shell is not a problem. But for the higher order isoparametric element, the displacements and their first derivates, were obtained by applying a constraint relating displacements at two hypotetical nodes, in the manner of Hibbitt and Marcal [16].

The shell was analysed first under elastic-plastic behavior; the results for imperfection parameters $\lambda=2$ and $\lambda=3$ are presented in Fig. 4 and 5, where we consider three pressure parameters $\rho=0.3$, 0.4 and 0.5 related to a critical value $p_{cr} = 0.15(t^2/R_1R_2)$, and the deflection parameter at the apex u_3/t is plotted against time. The shell is seen to have buckled when the deflection profile increases drastically for a small increment of pressure. It is important to mention that buckling occurs after the first maximum and not after a number of oscilations.

The problem of the externally pressurized imperfect hemisphere for the aluminum alloy (7075-T6) was first solved by Bushnell [17] for the estatic case, and by Marcal [18] for the elastic plastic case, and also by Marcal [9] for the elastic and elastic-plastic dynamic case, whose results are compared in Fig. 7. Based on these previous results; for the Concrete Elliptical Paraboloidal Shell, only the elastic-plastic dynamic case has been studied in this paper. Values of pressure parameters ρ which initiate buckling are plotted against the geometric parameter λ. For 1.5, the buckling pressure is governed very strongly by inestability of the material itself; so, for these values of λ any analysis neglecting nonlinear material and geometric behavior would be incorrect. The results are shown in Fig. 7a.

In computing the foregoing results, the equations were reassembled every ten increments, and corrected every second increment; this selection is based on the numerical experimentation presented by Marcal [9].

b) Creep buckling of the elliptical paraboloidal shell

The objective of this study is to find the creep buckling load for a life expectancy of 96 days, when subjected to various pressure levels.

The geometry of the shell is shown in Figs 2 and 3 with

f_1 = 2.75m, f_2 = 2.8m a = 13.70m, b = 13.45m, t = 0.06m, R_1=32.90m, R_2 = 33.57m and λ = 3.

The material is concrete with a compressive strength level f'_c = 150kg/cm^2 and a Poisson Ratio ν=0.15, which is assumed to be time independent for this study. The relaxation data were obtained from the creep test just mentioned.

The creep analysis has been done with pressure levels of 30%, 40% and 50% of the upper critical load of $0.15E(t^2/R_1R_2)$. The pressure was applied instantaneously using 10 load increments and then, sustained durint the creep process (fig. 8). In about 40 hr it was observed that the use of the out-of-balance force in the load vector makes the shell to approach the critical configuration; this force also cause over-corrections of equilibrium, and, at the end of the time step the stresses obtained were very small; when combined with the fading memory of the concrete the oscillations are set up; and for a given data of 96 hours the critical pressure parameter was found to be equal to 0.35.

CONCLUSIONS

a) The upper limit of the critical pressure for the elliptical paraboloidal concrete shell is $p_{cr} = 0.15(t^2/R_1R_2)$, and for the spherical aluminum alloy (7075-T6), or structural steel shell is $p_{cr} = 0.312E(t^2/R^2)$, [9]. It should not be $1.16\ E(t^2/R^2)$ [19].

b) The minimum unconfined compressive strength of the concrete should be in the structure above or equal to 250 kg/cm^2 (3500 psi).

c) In designing the elliptical paraboloidal concrete shell, one may see from Fig 7a that for values of λ between 1.5 and 3.5, the pressure parameter is, $p \doteq 0.35$, and the lower limit of the critical load is $(p_{cr})_L = 0.35 \times 0.15\ E(t^2/R_1R_2) = 0.053E(t^2/R_1R_2)$; therefore the design load should be as smaller as possible with respect to $(p_{cr})_L$.

d) In designing the spherical aluminum alloy (7075-T6), or structural steel shell, the lower limit of the critical load $(p_{cr})_L$ should be taken for the elastic-plastic dynamic case from Fig 7. For instance, for $\lambda = 3$, one obtains $\rho=0.49$, from which $(p_{cr})_L=0.49 \times 0.312E(t/R)^2 = 0.15E(t/R)^2$.

e) 100 hours after having removed the formwork, the deflection at the apex of the elliptical paraboloidal concrete shell should be smaller than 2 times its thickness t.

f) In the elliptical paraboloidal concrete shell, for values of the geometric parameter $\lambda<1.5$, the buckling pressure is governed very strongly by the unstable behavior of the material; so, for these values of λ, any analysis neglecting nonlinear material and geometric behavior would be incorrect; this could have been the cause of the collapses of this kind of shell in different countries.

g) The creep-buckling analysis was performed for $\lambda=3$, and its buckling pressure was of the same order of magnitude than the elastic-plastic dynamic case.

h) It is important to note that the practical consideration gave already the solution of the problem, but it is very important to know as deep as possible the theory, because, as the author may state: "A good practice should be based in a very good and clear knowledge of the theory".

R E F E R E N C E S

[1] Chen, C.T.A. and Chen, W.F., "Constitutive relations for concrete", "Journal Engineering Mechanics Division, ASCE, AUGUST, 1975.

[2] Ballesteros, P., and Alamo, R. "Ecuaciones constitutivas del concreto", División de Estudios Superiores, Fac. Ingeniería, National University of México, 1977.

[3] Bažant, Z.P. and Osman, E., "Double-power law for basic creep of concrete" *Materials and Structures* (Rilem, París) Vol. 9, 1976, Nª 49.

[4] Larsen, P.K. and Popov, E.P. "Large displacement analysis of viscoelastic shells of revolution", *Computer methods in Applied Mechanics and Engineering* 3(1974) 237-253, North Holland Publishing Co.

[5] Truesdell, C. and Noll, W., "The nonlinear field theories of mechanics", in: S. Flügge (ed), *Handbuch der Physik;* III/3 (1965).

[6] Fredrickson, A.G., "Principles and applications of Rheology" *Prentice Hall*, 1964.

[7] Oden, J.I., "A generalization for the finite element concept and its application to a class of problems in nonlinear viscoelasticity", in: *Developments in theoretical and Applied Mechanics IV, D.* Frederick (ed.) (Pergamon, 1968) 581-592.

[8] McNamara, J.F., "Incremental Stiffness method for Finite Element Analysis of the Nonlinear Dynamic Problem", PhD. Thesis, submitted August 1971.

[9] Zienkiewicz, O.C., Gallagher, R.H. and Marcal, P.V., "Advanced Topics in Finite Element Analysis", Newport, R.I., July 21-25, 1975, Marc Analysis Research Corporation

[10] Marcal. P.V. and King, I.P., "Elastic-plastic analysis of two-dimensional stress system by the finite element method" *International Journal of Mechanical Science*, 9, No. 3, 1967, pp. 143-155.

[11] Hibbitt, H.D., Marcal, P.V. and Rice, J.R., "A finite element formulation for problems of large strain and large displacement", *International Journal of Solid and Structures*, 6, pp. 1069-1970.

[12] Houbolt, J.C. "A recurrence matrix solution for the dynamic response of elastic aircraft" *Journal of Aerospace Sciences*, 17, 1950, pp. 540-550.

[13] Haisler, W.E., Stricklin, J.A. and Stebins, F.J., "Development and evaluation of solution procedures for geometrically non-linear structural analysis by the direct stiffness method", *AIAA/ASME 12th Structures, Structural Dynamics and Material Conference*, Anaheim, California, April 19-21, 1971.

[14] Klein, S. and Sylvester, R.J., "The linear elastic dynamic analysis of shells of revolution by matrix displacement method", Air Force Flight Dynamics Laboratory, TR-66-80, 1966, pp. 299-329.

[15] Khojasteh-Bakht, M., "Analysis of elastic-plastic shells of revolution under axisymmetric loading by the finite element method", Ph. D. dissertation, University of California at Berkeley, SESM 67-68, April 1969..

[16] Hibbit, H.D. and Marcal, P.V., "Hybrid finite element analysis with particular reference to axisymmetric structures", *Proc. AIAA 8th aerospace science meeting*, New York, January

19-21, 1970.

[17] Bushnell D., "Nonlinear axisymmetric behavior of shells of revolution", *AIAA Journal*, 5 No 3, 1967, pp 432-439

[18] Marcal, P.V., "Finite element analysis of combined problems of nonlinear material and geometric behavior", *Proc. ASME, Joint computer conference on computational approach to applied mechanics*, Chicago, 1969.

[19] Ballesteros, P. "Congress of Mexico. The application of shell structures. General Report. Theme IV", *Bulletin No. 41, IASS*, 1969.

[20] Timoshenko, S.P. and Gere, J. "Theory of elastic stability", *McGraw Hill Book Co.*,1962.

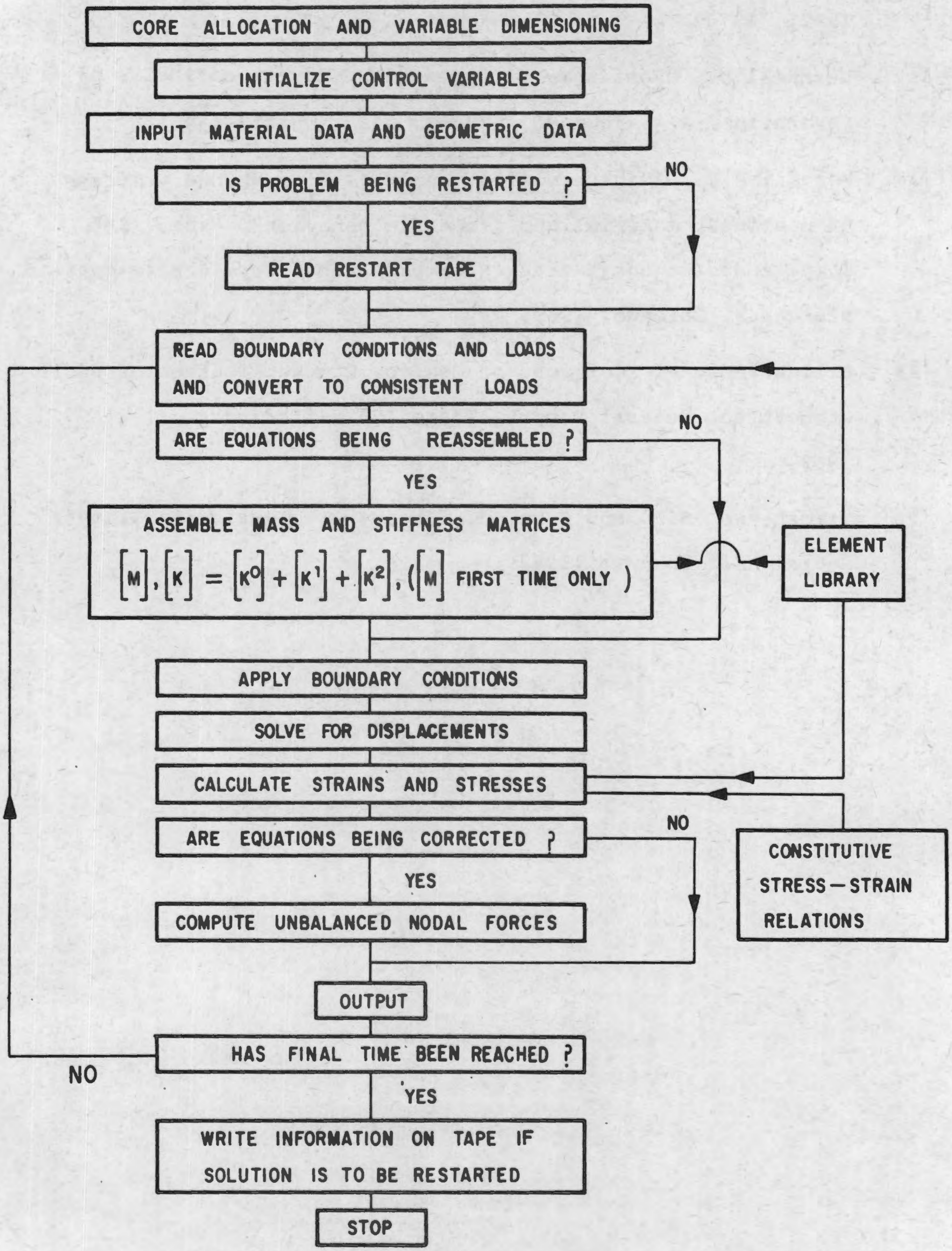

Fig 1 Flow chart for computer program

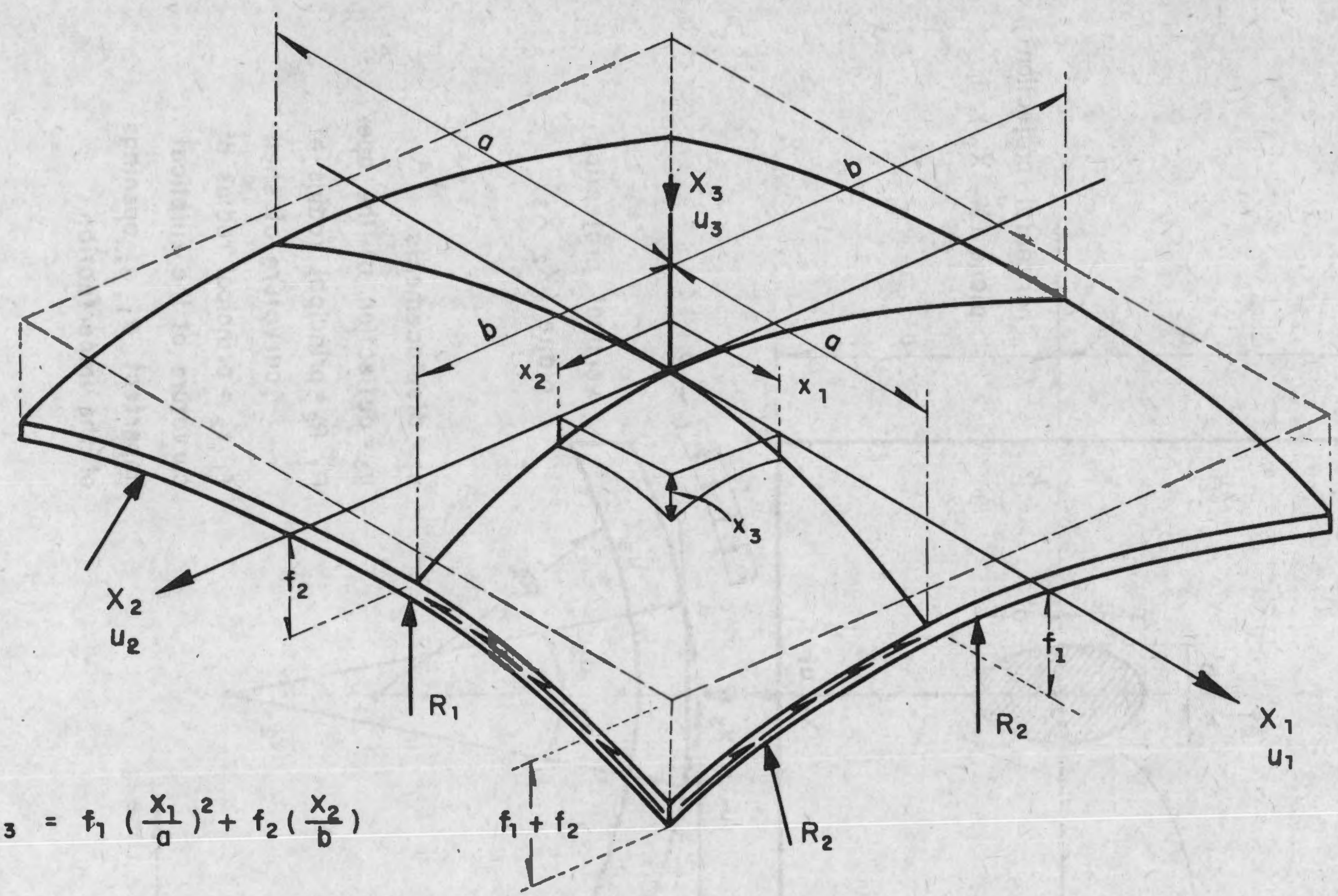

$$X_3 = f_1 \left(\frac{X_1}{a}\right)^2 + f_2 \left(\frac{X_2}{b}\right)$$

This surface is generated by moving a parabolic curve along another parabola, any plane parallel to plane (X_1 X_2) intersects the surface in an ellipse, and any plane parallel to (X_1 X_3) or (X_2 X_3) intersects the surface in a parabola

Fig 2 Geometry of the elliptical paraboloidal shell supported by tangential shear along the boundary

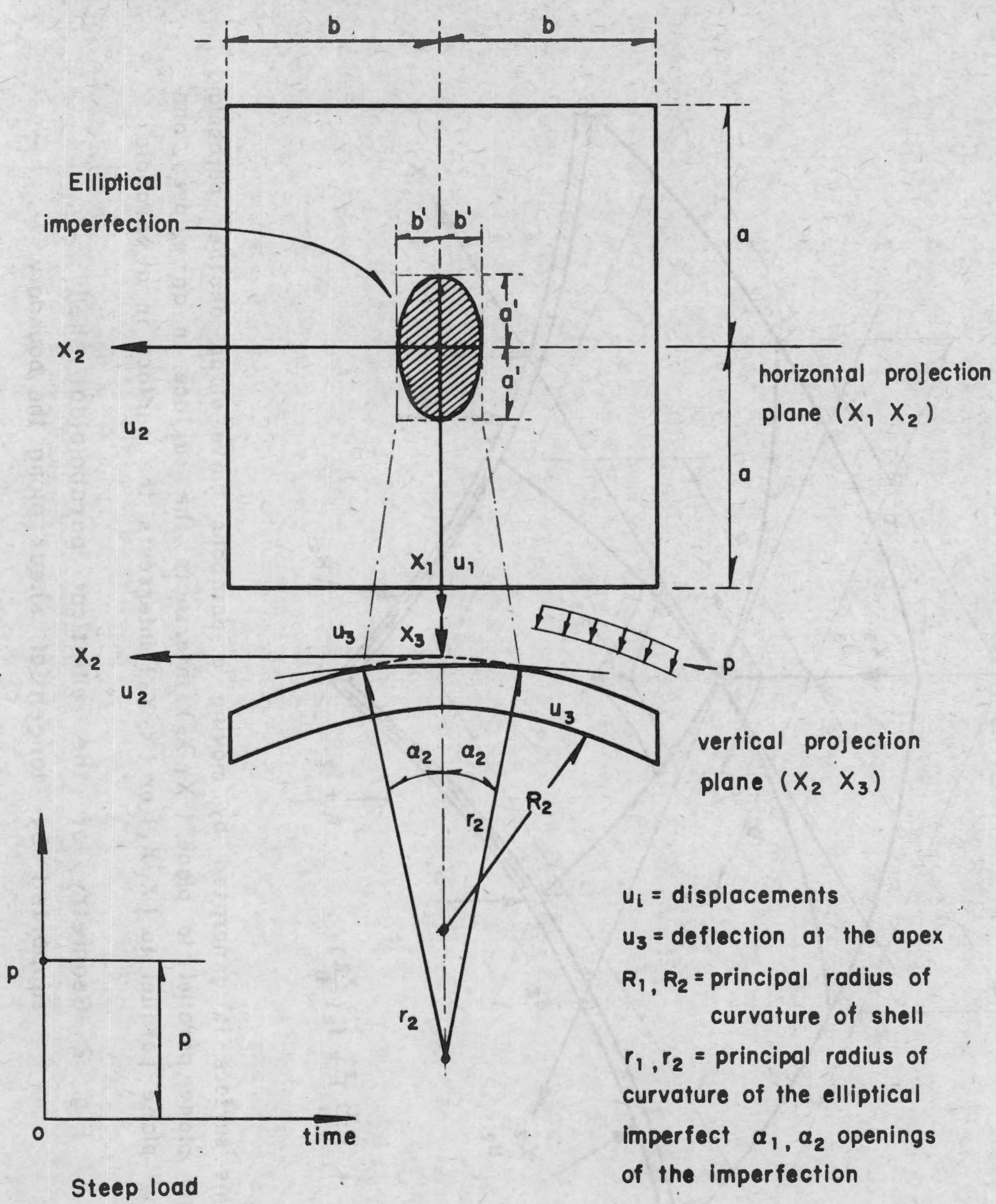

Fig 3 Elliptical imperfection at the origin of the elliptical paraboloid shell with a radius of curvature r_1 and r_2

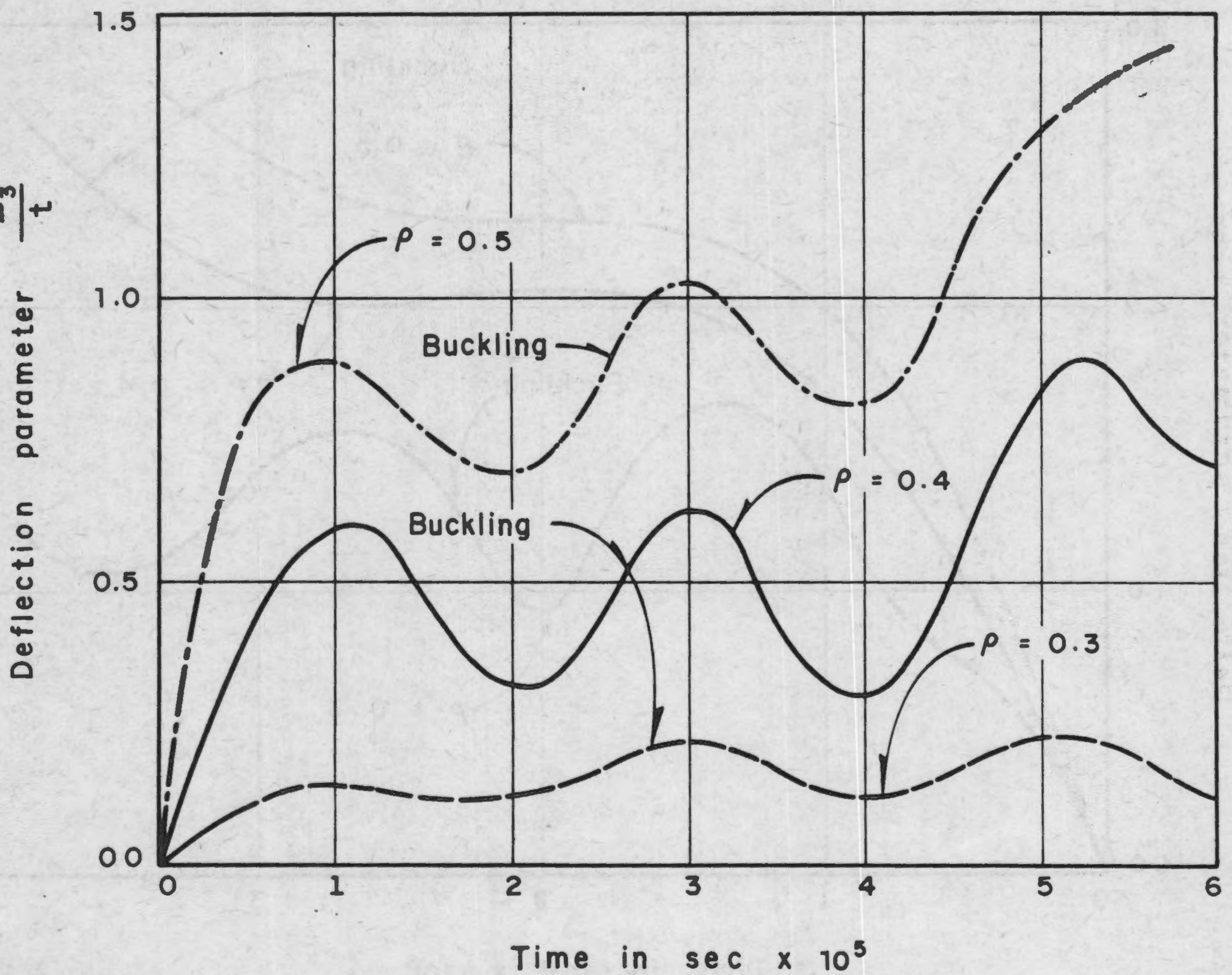

Fig 4 Deflection profiles for elastic - plastic buckling of imperfect elliptical paraboloidal shell with $\lambda = 2$ ($\Delta T = 2.5 \times 10^{-6}$ sec)

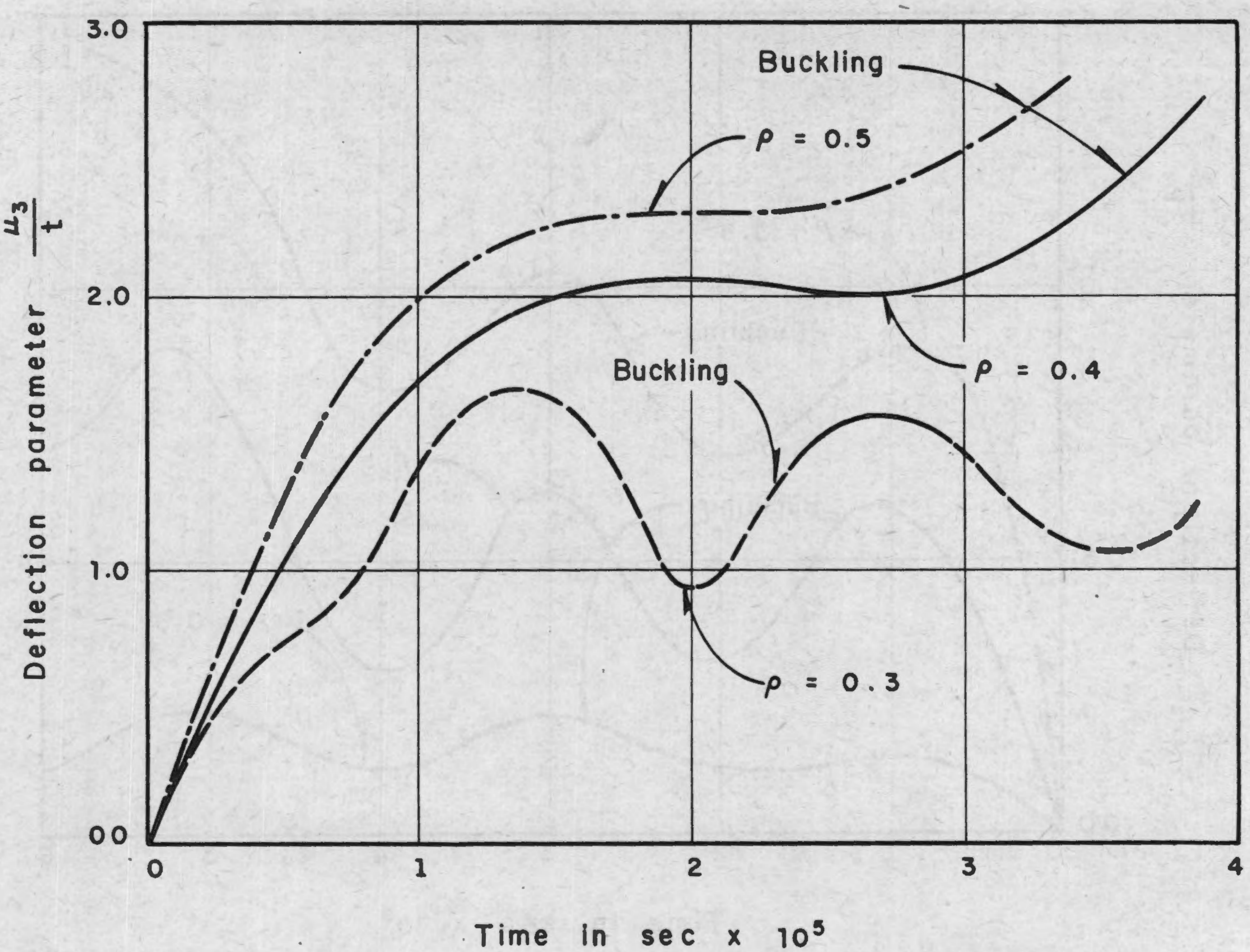

Fig 5 Deflection profiles for elastic - plastic buckling of imperfect elliptical paraboloidal shell with λ = 3

Model of stress - strain curve :

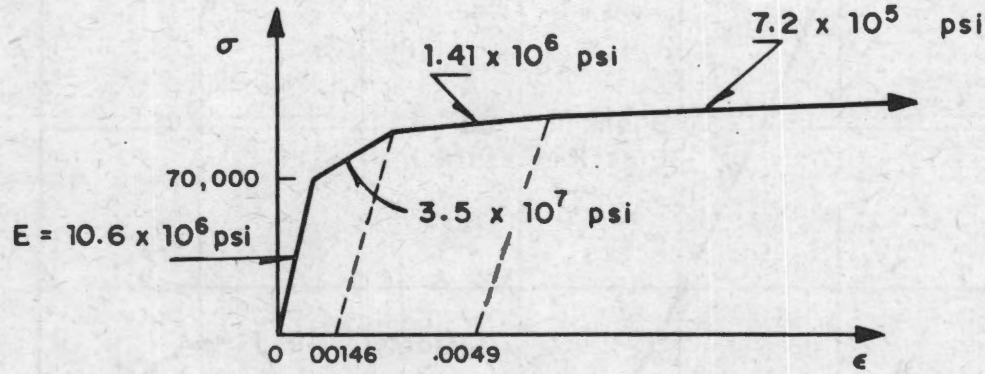

Inperfection parameter $\lambda = \left[12 (1 - \nu^2) \right]^{1/4} \left(\frac{R}{t}\right)^{1/2} \left(\frac{R}{r}\right)^{1/2} \alpha$

Upper limit of critical pressure $p_{CR} = 0.312 \; E \left(\frac{t}{R}\right)^2$

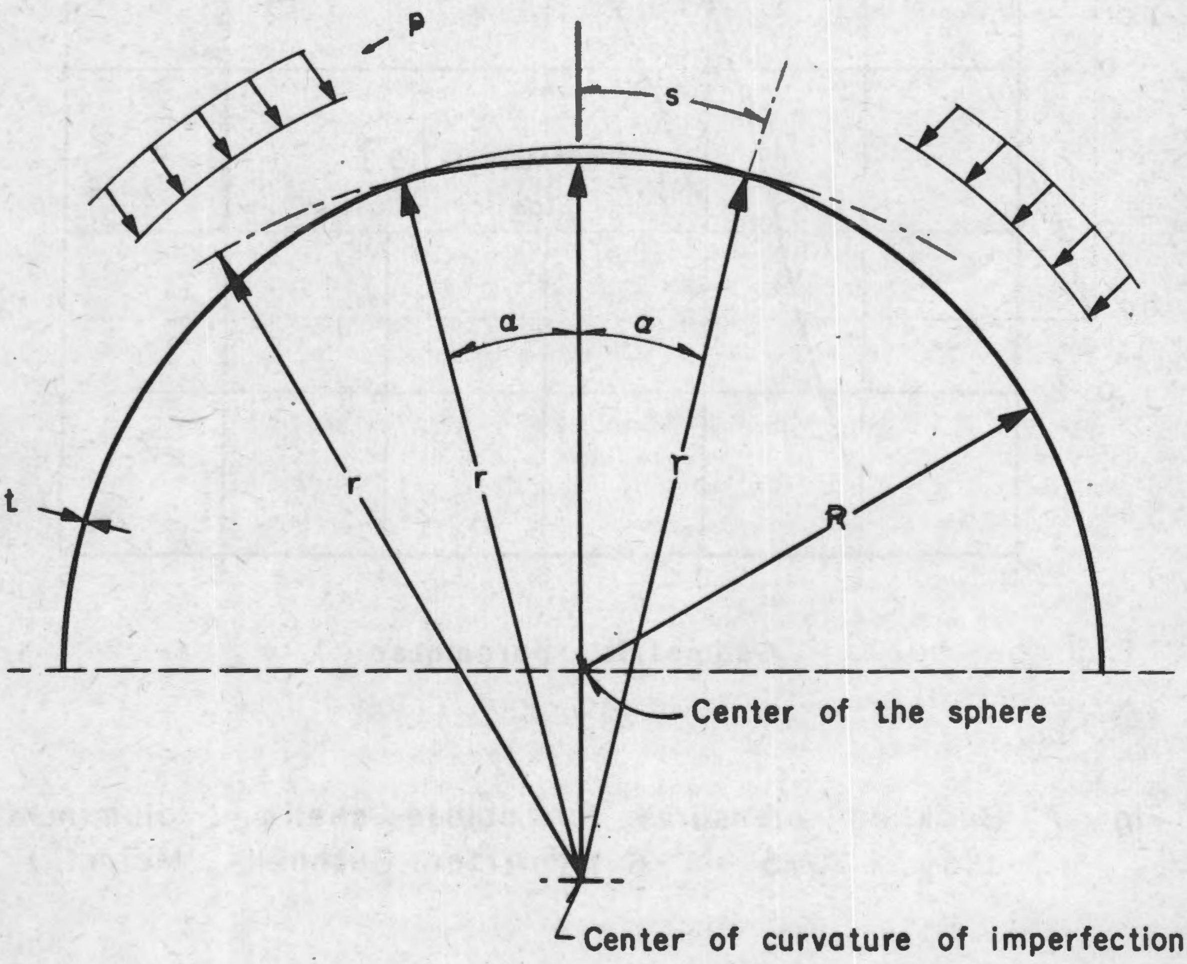

Fig 6 Externally pressurized imperfect hemisphere and material constants , for aluminum alloy (7075 T-6)

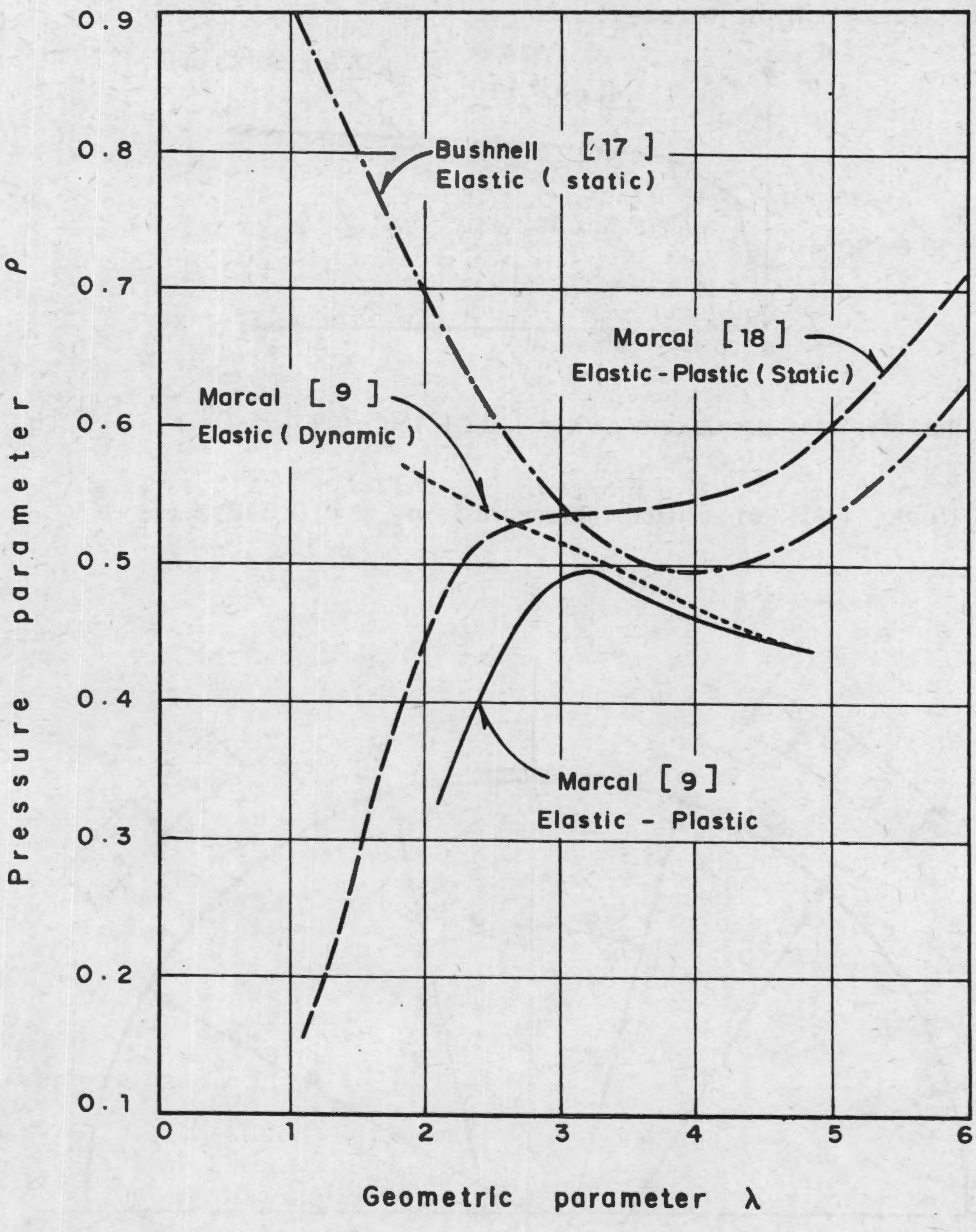

Fig 7 Buckling pressures for oblate shells, aluminum alloy (7075 - T-6) (After Bushnell, Marcal)

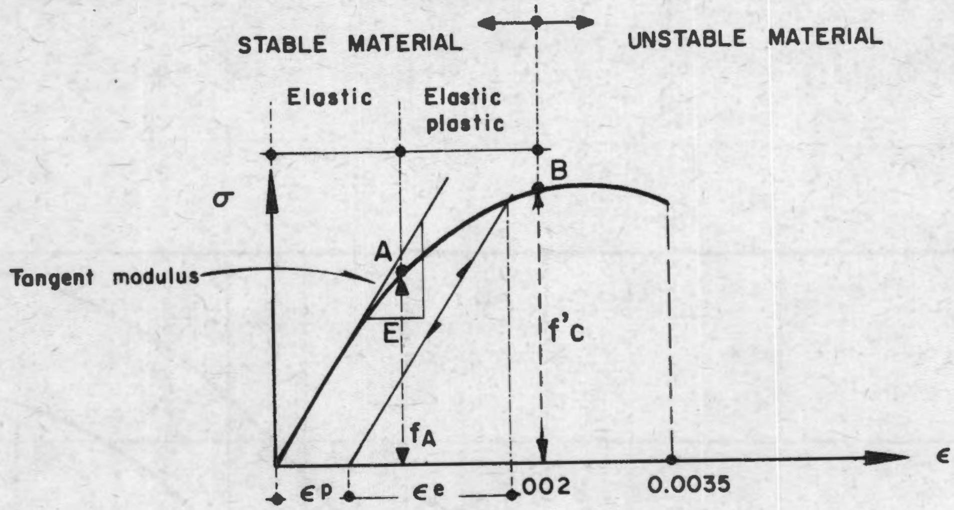

Model of stress – strain for concrete

Geometric parameter $\lambda = 1.84 \left(\frac{R_1+R_2}{2\,t}\right)^{1/2} \left(\frac{R_1+R_2}{r_1+r_2}\right) \left(\frac{\alpha_1+\alpha_2}{2}\right)$

Upper limit of critical load $p_{CR} = 0.15\ E\ \frac{t^2}{R_1\ R_2}$

f_A = Limit of elasticity $\doteq 0.5\ f'_c$

f'_c = Limit of plasticity for $\epsilon \leq 0.002$

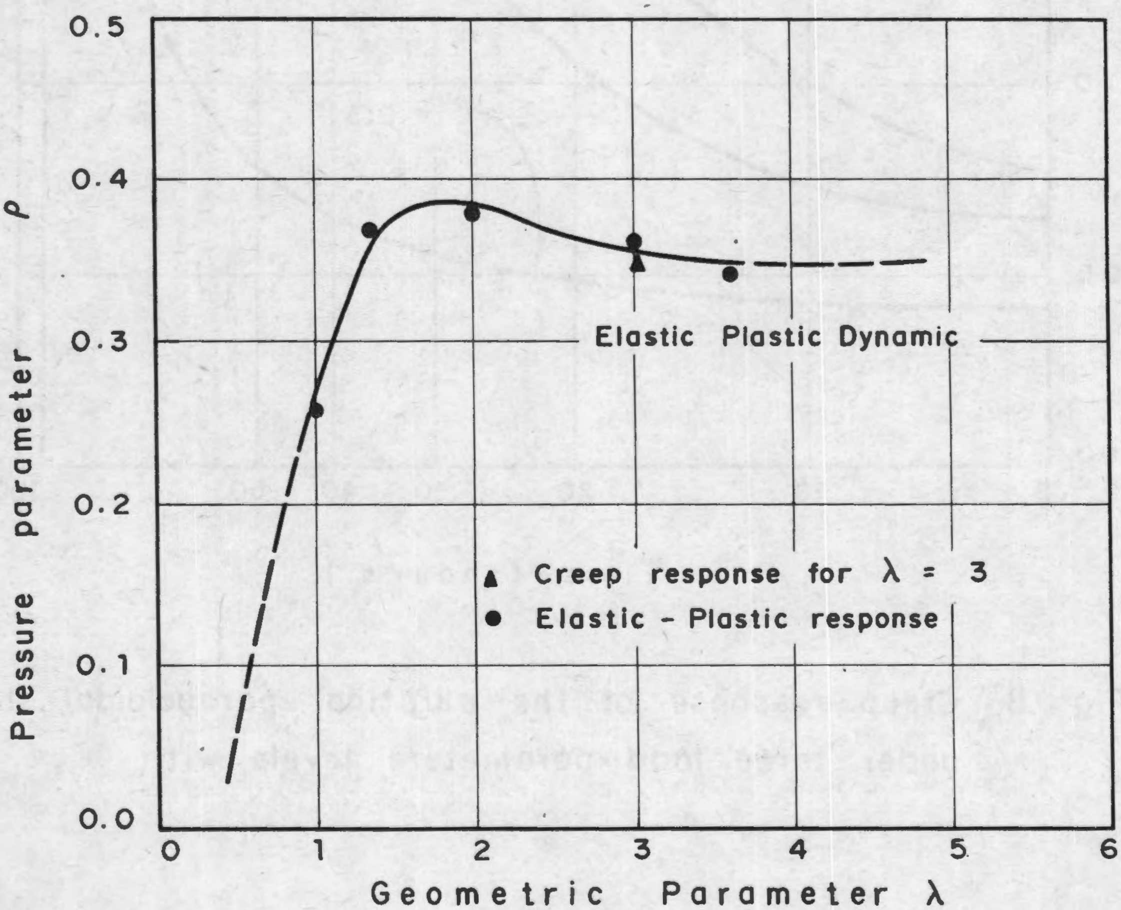

Fig 7 a Buckling pressures for oblate elliptical paraboloidal concrete shells

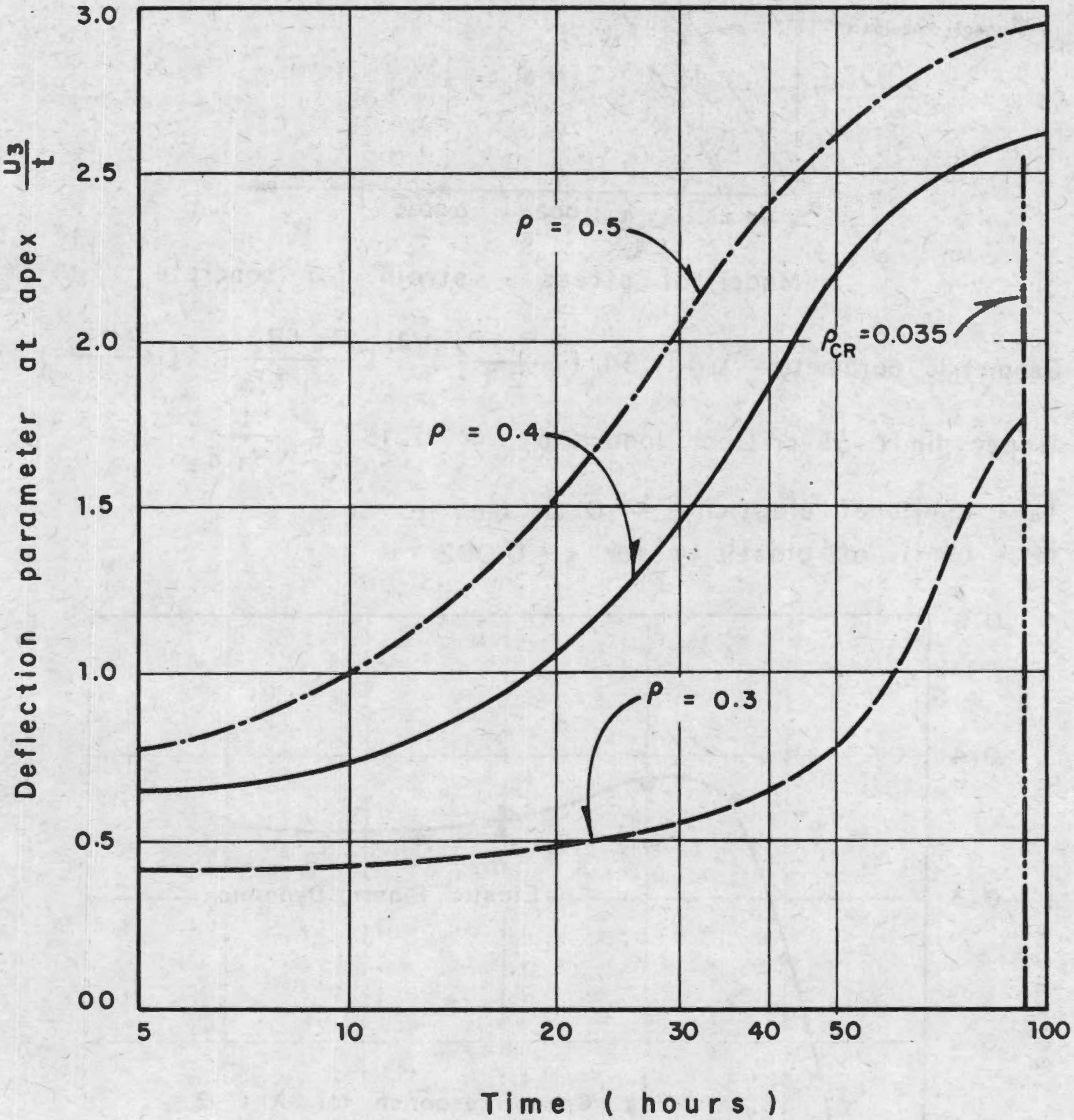

Fig 8 Creep response of the elliptical paraboloidal shell under three load parameters levels with λ = 3

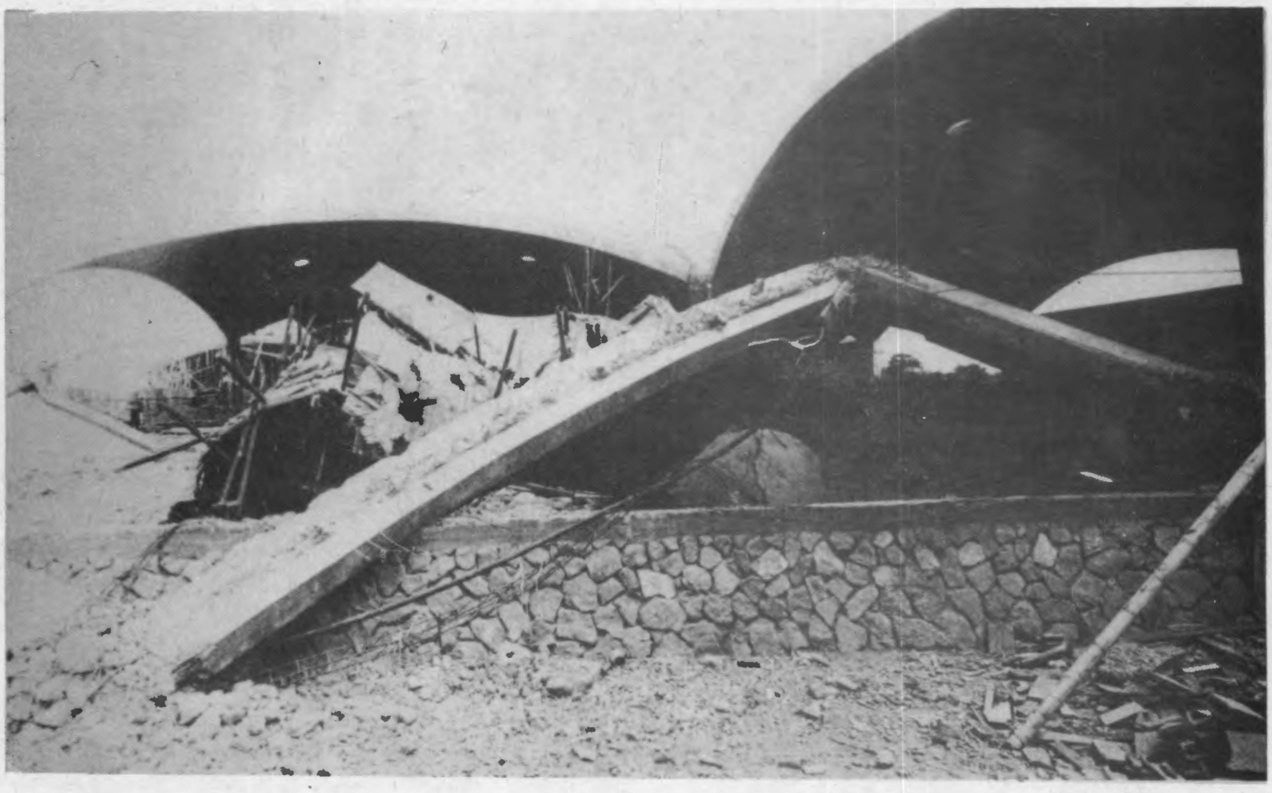

Fig 9

Collapse of the elliptical paraboloidal concrete shells

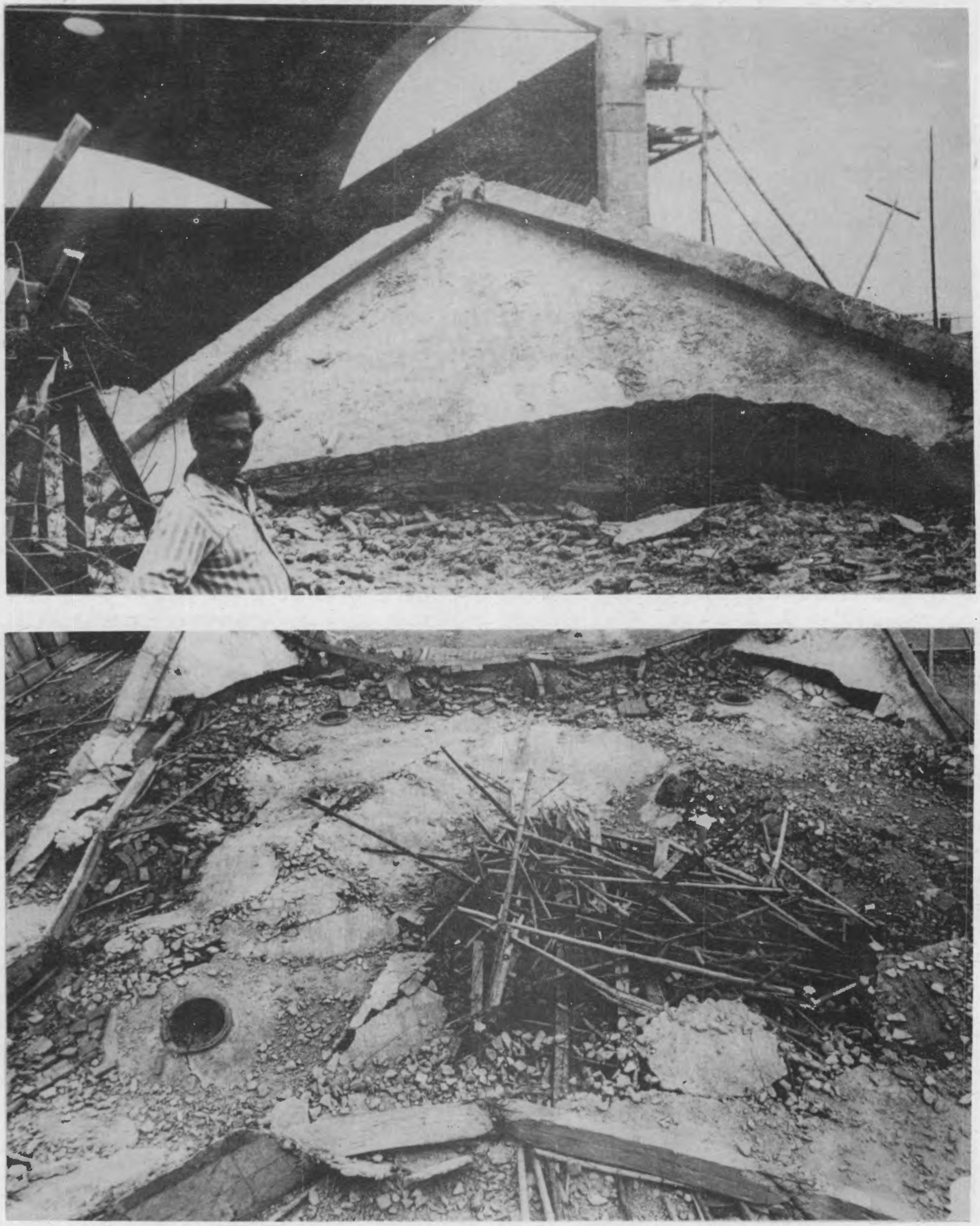

Fig 10

Collapse of the elliptical paraboloidal concrete shells

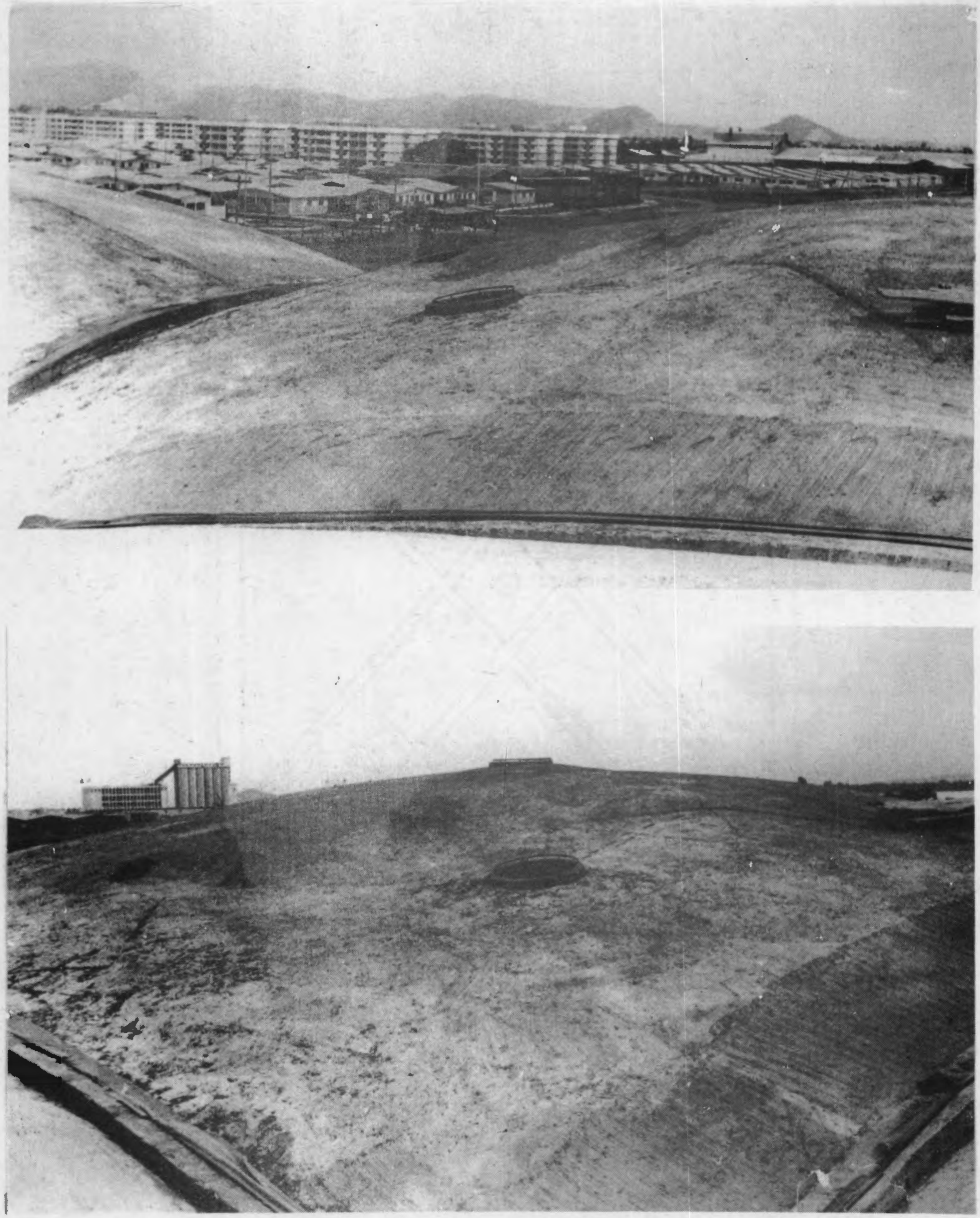

Fig. 11

Geometric Imperfection for the elliptical paraboloidal concrete shells

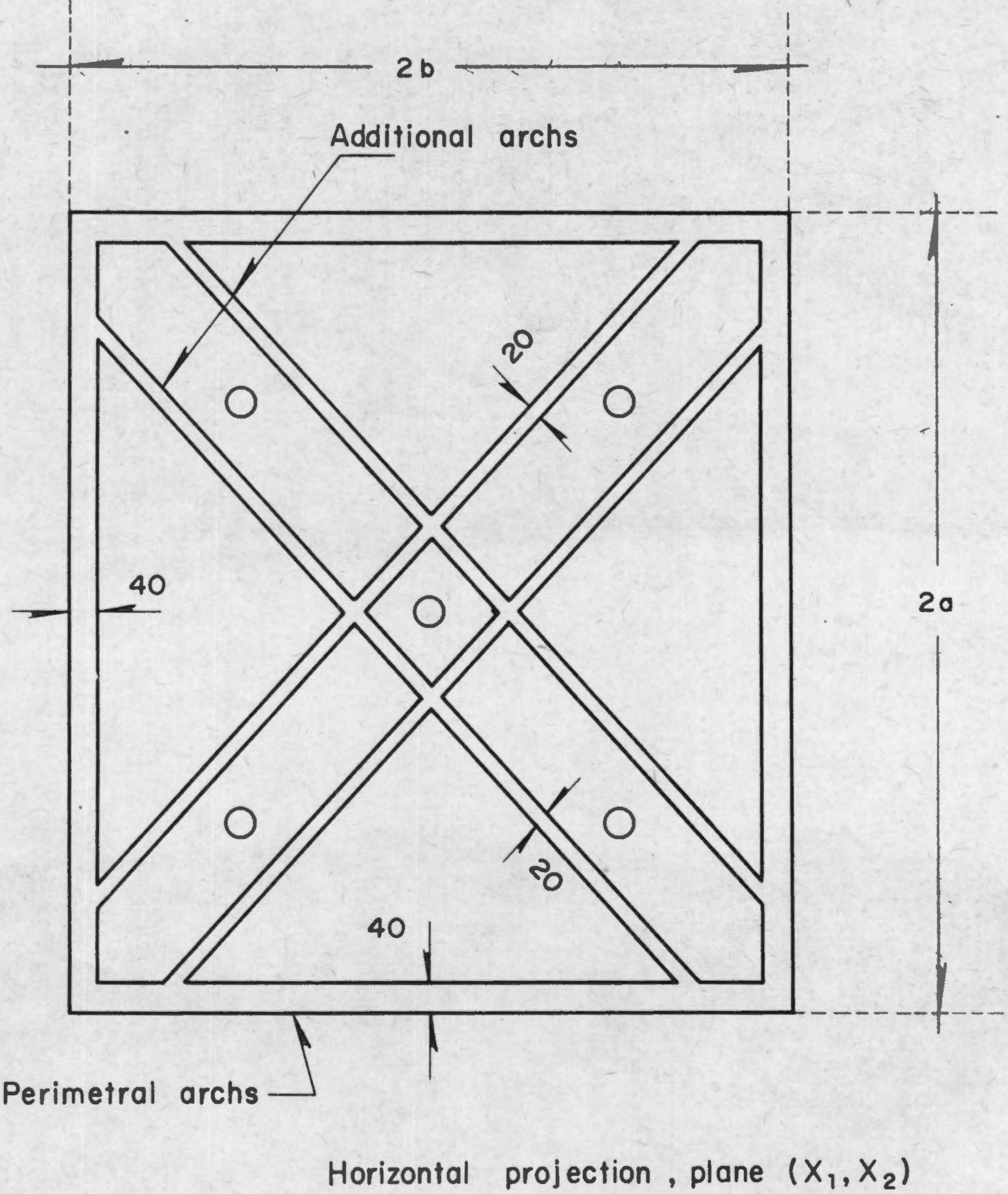

Fig 12 Additional concrete arches for increasing buckling capacity of the shell

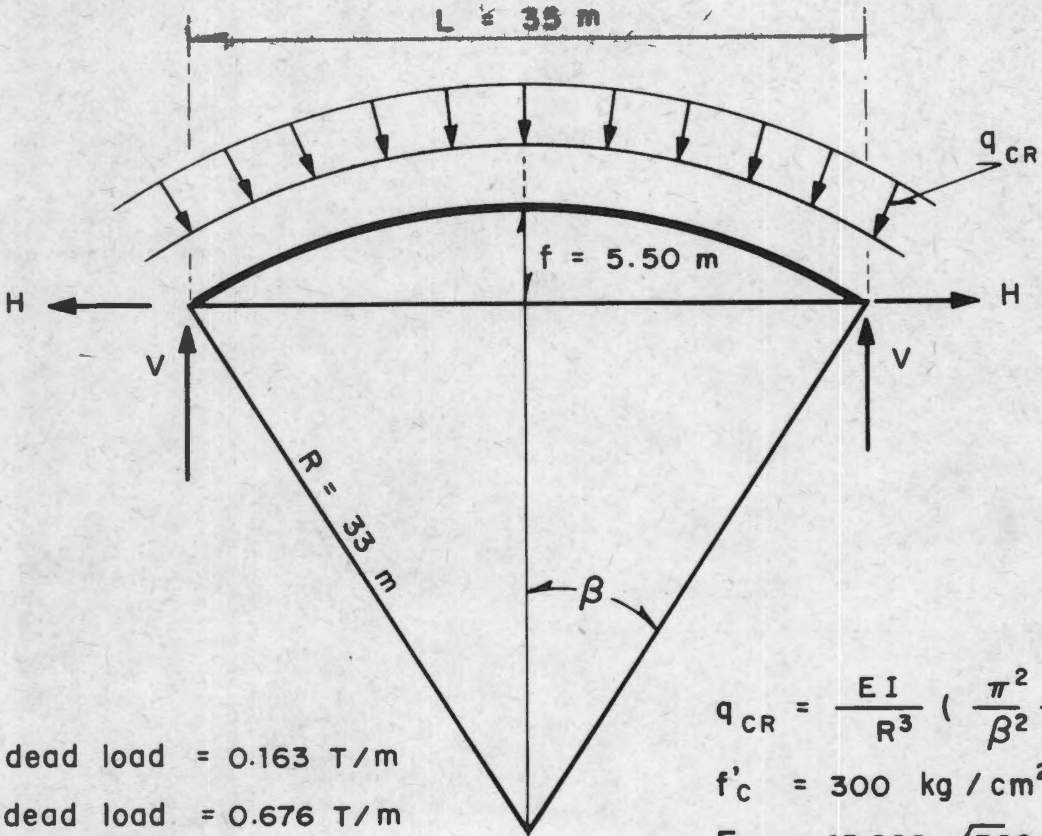

Arch dead load = 0.163 T/m

Shell dead load = 0.676 T/m

Live load = 0.175 T/m

$\sum$ = 1.014 T/m

Buckling coef. ≐ 2.5

$$q_{CR} = \frac{EI}{R^3}\left(\frac{\pi^2}{\beta^2} - 1\right), \text{ Ref. } [20]$$

$f'_c = 300 \text{ kg/cm}^2$

$E_c = 15\,000\sqrt{300} = 259\,807$ kg/cm

$I = \frac{1}{12} \times 20 \times \overline{40}^3 = 106\,667 \text{ cm}^4$

$R = 3\,300$ cm ; $\beta = 0.55$ radians

$q_{CR} = 2\,438$ kg/m

Fig 13 Buckling capacity of additional arches

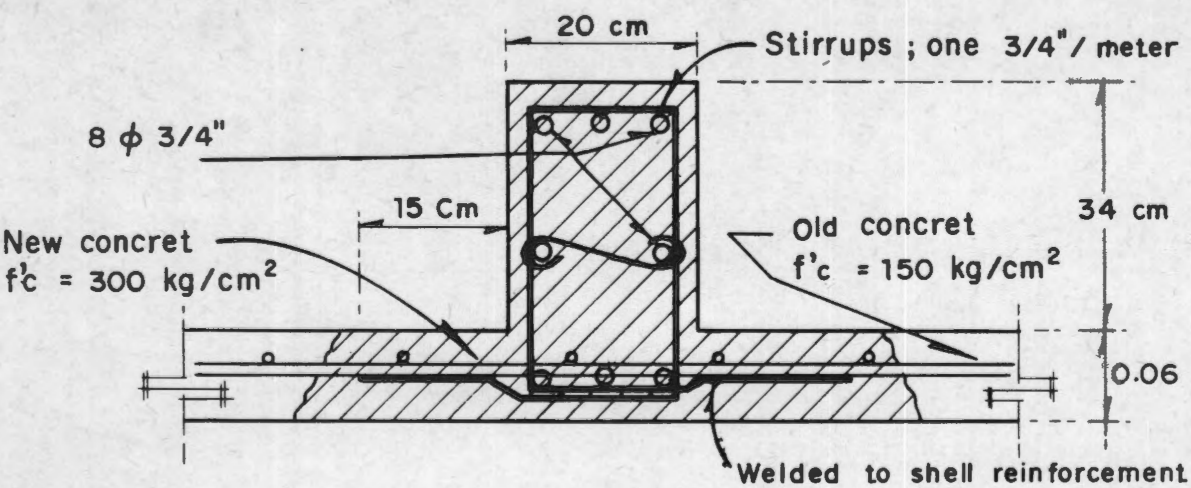

Fig 14 Connection between the arch and the existing shell

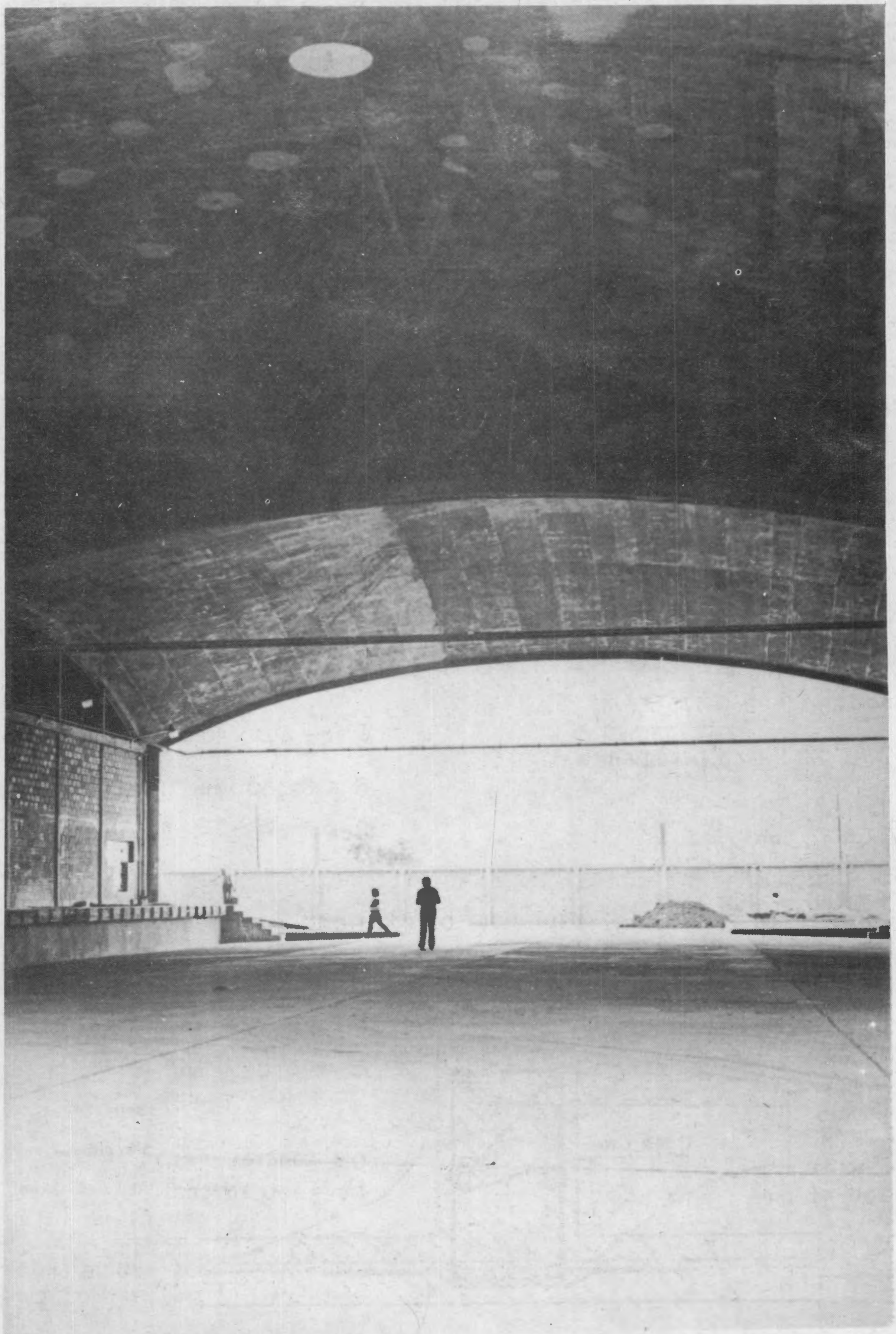

Fig 15

A view from the interior of the connection between additional arches and shell

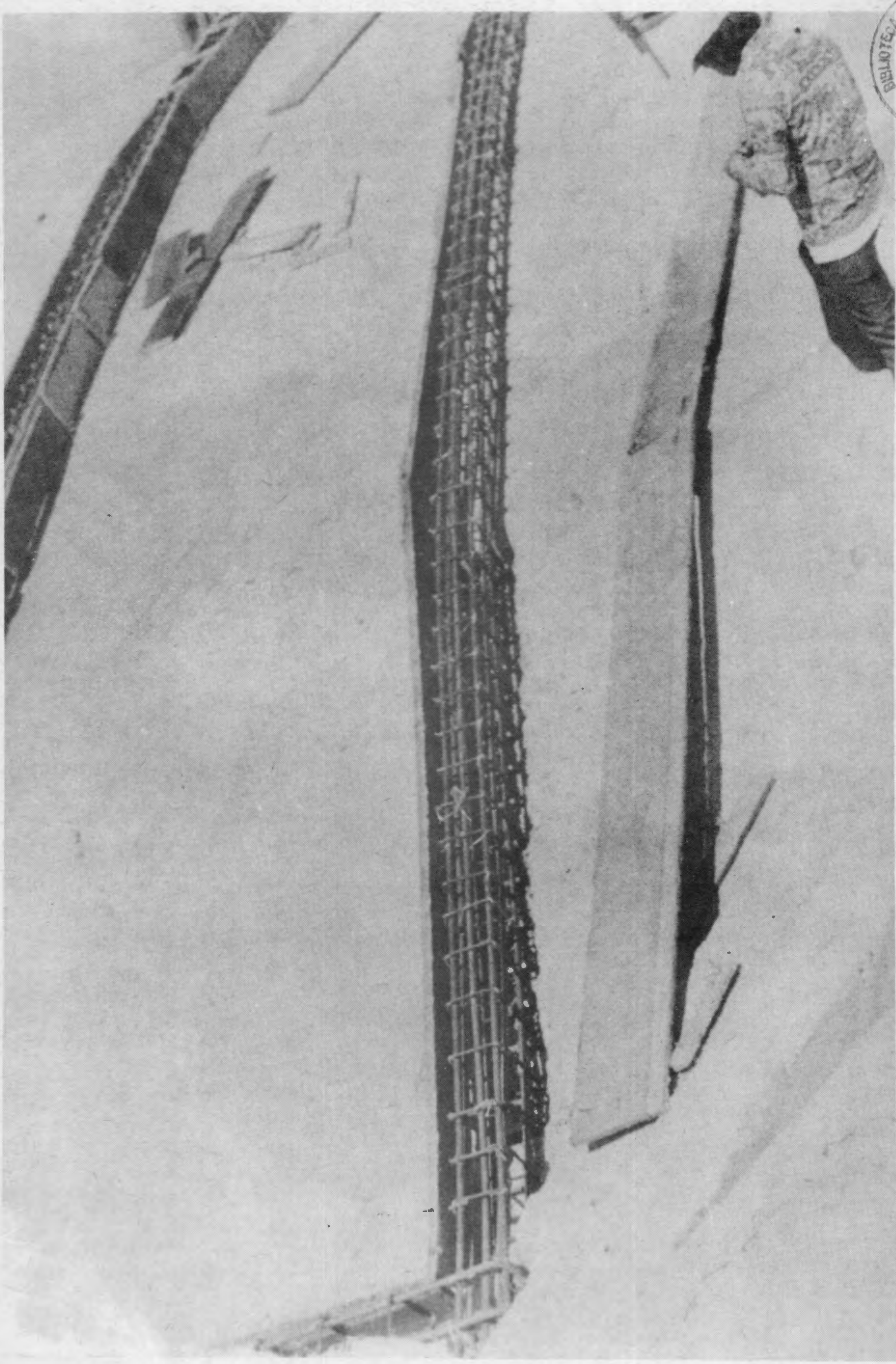

Fig 16

The additional arches, for increasing the buckling capacity of the shell.

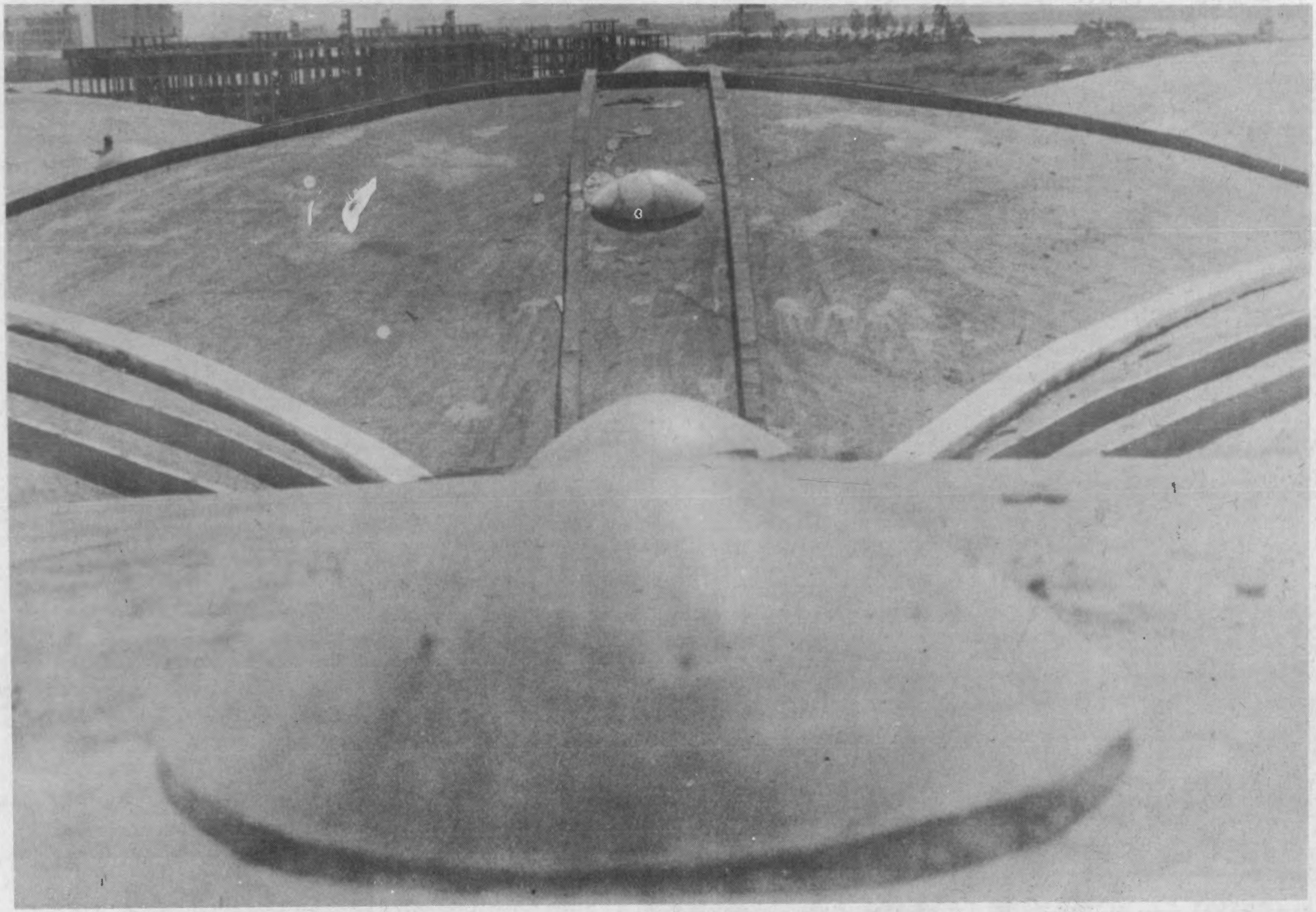

Fig 17

The additional arches, for increasing the buckling capacity of the shell.

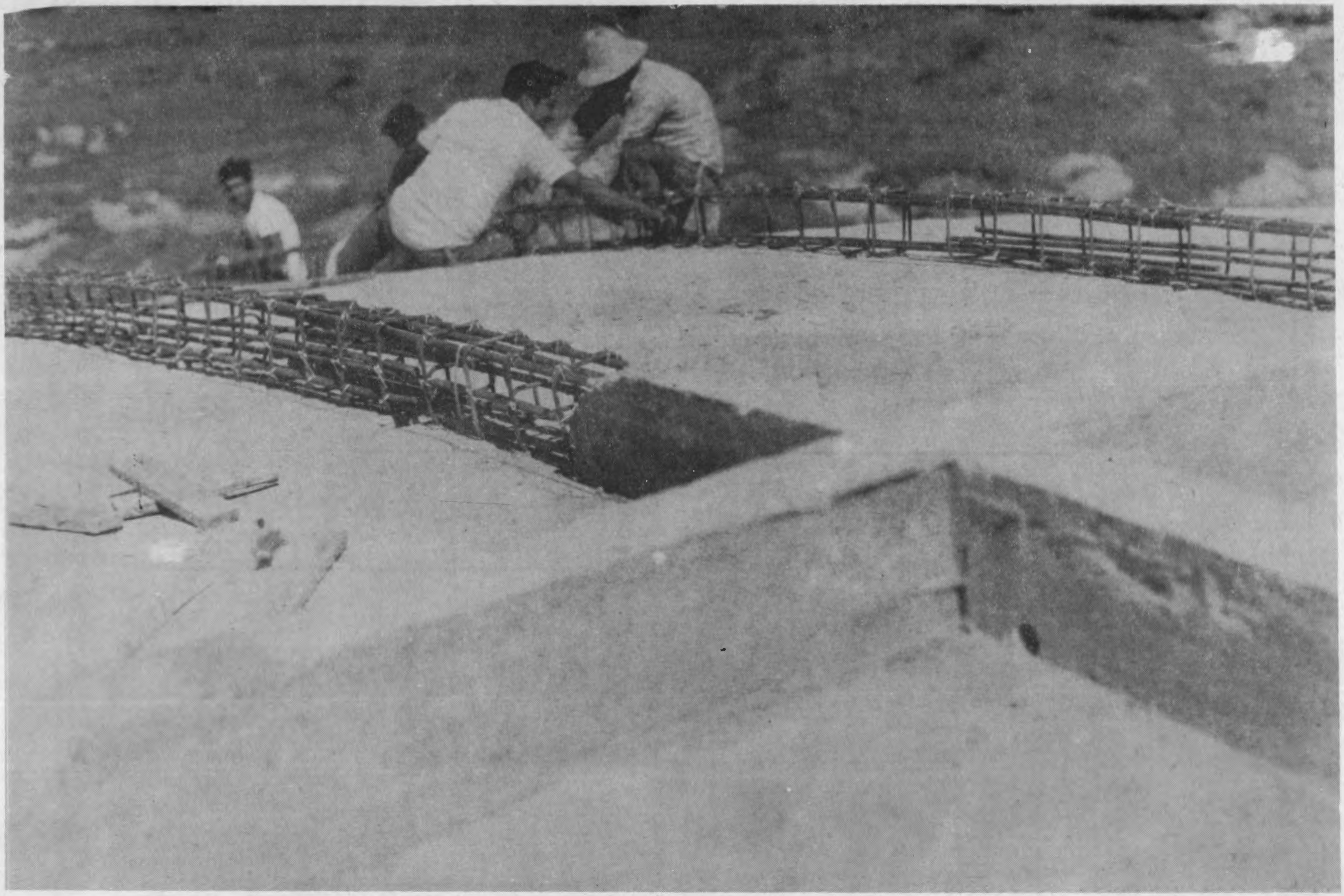

Fig 18

The additional arches, for increasing the buckling capacity of the shell.

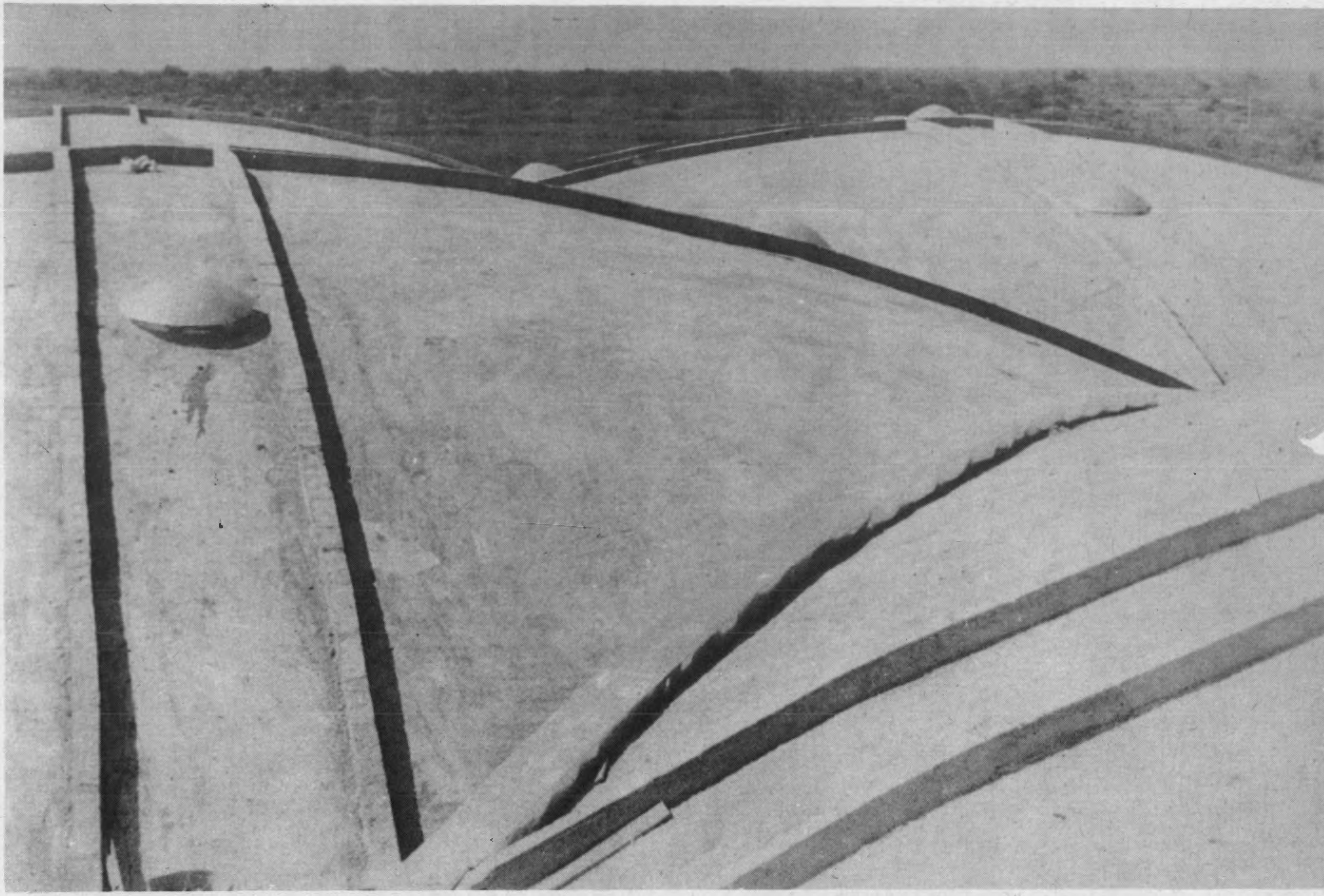

Fig 19 The additional arches, to increase the buckling capacity of the shell.